Journal of Medicinal Chemistry Article

J. Med. Chem. **2010,** *53,* 155–165 **155**
DOI: 10.1021/jm9015284

The Discodermolide Hairpin Structure Flows from Conformationally Stable Modular Motifs

Ashutosh S. Jogalekar,[†] Frederik H. Kriel,[†] Qi Shi,[†] Ben Cornett,[†] Daniel Cicero,[‡] and James P. Snyder*,[†]

[†]*Department of Chemistry, Emory University, 1515 Dickey Drive, Atlanta, Georgia 30322, and* [‡]*Faculty of Chemical Sciences and Technologies, University of Rome "Tor Vergata", 00173 Rome, Italy*

Received May 31, 2009

(+)-Discodermolide (DDM), a polyketide macrolide from marine sponge, is a potent microtubule assembly promoter. Reported solid-state, solution, and protein-bound DDM conformations reveal the unusual result that a common hairpin conformational motif exists in all three microenvironments. No other flexible microtubule binding agent exhibits such constancy of conformation. In the present study, we combine force-field conformational searches with NMR deconvolution in different solvents to compare DDM conformers with those observed in other environments. While several conformational families are perceived, the hairpin form dominates. The stability of this motif is dictated primarily by steric factors arising from repeated modular segments in DDM composed of the C(Me)-CHX-C(Me) fragment. Furthermore, docking protocols were utilized to probe the DDM binding mode in β-tubulin. A previously suggested pose is substantiated (Pose-1), while an alternative (Pose-2) has been identified. SAR analysis for DDM analogues differentiates the two poses and suggests that Pose-2 is better able to accommodate the biodata.

Introduction

(+)-Discodermolide (DDM, **1**[a]), a polyketide macrolide isolated from the marine sponge *Discodermia dissolute*,[1] inhibits the cellular action of microtubules by stabilizing them. The most potent promoter of microtubule assembly known, DDM binds to the taxane binding site on the β-subunit of tubulin.[2] Recently, the compound was withdrawn from clinical trials following indications of pulmonary toxicity.[3] However, the quest for nontoxic discodermolide analogues that preserve potency remains an active pursuit.[4]

Design of such analogues would benefit from knowledge of the conformation of DDM residing in the binding pocket of microtubules and associated stabilizing factors. Two groups have investigated the binding conformation of the drug experimentally, most notably by means of transferred NOE NMR spectroscopy.[5,6] The conformation derived from these experiments is very similar to the solid-state conformation[1,7] and to a single structure proposed in CD_3CN solution.[8] In this respect, in spite of 15 easily rotated single bonds along its main chain, discodermolide appears to be unique among protein ligands in its display of deceptive inflexibility. In the present work, the conformations of DDM have been investigated by performing multiple molecular mechanics conformational searches and taking advantage of the NMR Analysis of Molecular Flexibility in Solution methodology[9,10] (NAMFIS) to deconvolute the averaged NMR spectrum of DDM in DMSO-d_6 and D_2O and, thereby, obtain estimates of the Boltzmann populations of rotational isomers in solution. We find that the conformations determined in the solid-state and proposed in solution are strongly represented in the computationally generated ensembles and NAMFIS families. In a previous report, Smith and coworkers performed an efficient triply convergent gram-scale synthesis of (+)-discodermolide by employing the common polypropionate precursor **2**, a synthon carrying three contiguous stereogenic carbons and appearing three times in **1**.[4c,7] The strategy was subsequently employed by a Novartis team in a 60 g preparation of the same compound for clinical study.[11] Smith et al. have likewise discussed the NMR spectrum of DDM in terms of $A^{1,3}$ strain and *syn*-pentane interactions as they contribute to shaping the dominant solution conformation of DDM in acetonitrile-d_3.[8] The outcome was foreshadowed by the conformational principles laid down by Hoffmann and coworkers.[12,13] The present study reinforces as well as adds to the previous discussions in four distinct ways by (1) highlighting the dominance of steric interactions in the multiconformational DDM solution ensemble, (2) applying quantum chemical density functional (DFT) calculations and comparative conformer energetics to examine the surprising persistence of conformational integrity in solution, the solid-state and at the tubulin binding site, (3) proposal of a new binding mode for (+)-discodermolide on β-tubulin, and (4) suggesting it to be favored in terms of the drug's bioactive conformation and SAR.

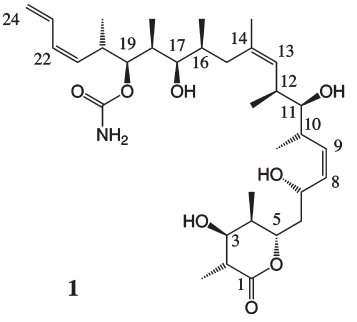

1

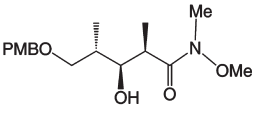

2

Results and Discussion

Conformational Searching. Conformational sampling and refinement gave a total of 1282 unique conformations across

*To whom correspondence should be addressed. Phone: 404-727-2415. Fax: +1-404-727-6586. E-mail: jsnyder@emory.edu.

[a] Abbreviations: DDM, discodermolide; PTX, paclitaxel; SAR, structure−activity relationship; DMSO, dimethyl sulfoxide; MM3*, MMFFs, OPLS2005, OPLS-AA, and AMBER, various molecular mechanics methods; MM-GBSA, molecular mechanics generalized Born surface area; ROESY, rotating-frame NOE spectroscopy; NAMFIS, NMR analysis of molecular flexibility in solution; DFT, density functional theory; rmsd, root-mean-square deviation; SSD, sum of square differences; PDB, protein data bank.

Published on Web 11/06/2009

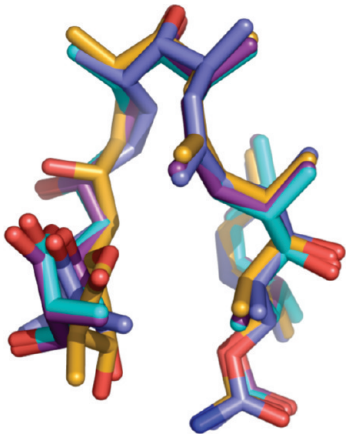

Figure 1. Superposition of the global minima from the four force fields: AMBER (blue), MMFFs (cyan), OPLS2005 (gold), and MM3* (purple). The lactone is at lower left.

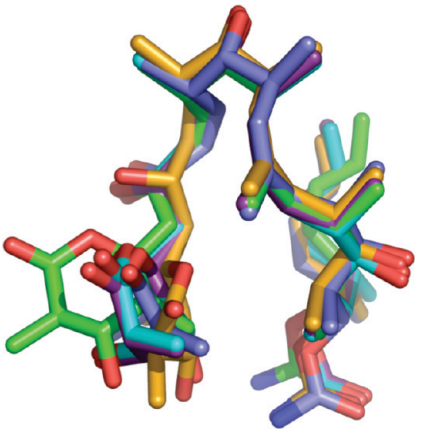

Figure 2. Superposition of the four force field global minima and the crystal structure[15,16] (green) of discodermolide.

four well-established force fields. Examination of the global minima from the four methods shows them to be surprisingly similar. This observation is striking in light of the disparate parametrization criteria and charge models used by different molecular mechanics methods to determine energy minima for flexible molecules.[14] Figure 1 superposes the four structures with an average all heavy-atom rmsd of only 0.9 Å. The main variability is in the disposition of the lactone side chain. The four global minima are also very similar to the DDM X-ray structure[1] as displayed in the superposition of Figure 2. The crystal structure (green) presents the lactone in a different orientation compared to the force field structures.

Given that modern force fields are formulated with commonly employed equations and parameters designed to mimic experimental structure and relative energies where known, naïve application to a new system can lead to two expectations that frequently do not accord with experiment. First, low energy conformations (e.g., ≤ 3 kcal/mol) may not be experimentally viable but produced by a force field as a result of overstabilizing electrostatic interactions.[14] Second, a calculated global minimum is frequently force field dependent, different structures arising from the characteristics of the specific equations and the accompanying parameters. For example, the extensive conformational sampling of Perola and Charifson[17] led to the result that numerous drug-like molecules are predicted to have substantially different global minima when evaluated with the highly regarded MMFF and OPLS-AA molecular mechanics methods. As a result, the calculated global minima depicted by Figures 1 and 2, while highly suggestive, cannot be taken at face value.

Deconvolution of the DDM Time-Averaged NMR Spectrum in DMSO-d_6. A previous DDM NAMFIS study in DMSO-d_6 from this laboratory identified several conformational families with the X-ray conformation as a minor contributor to the solution ensemble.[18] Because that work employed only a single force field, and subsequent experimental work has persistently favored the hairpin conformation for the drug, the NAMFIS evaluation has been repeated here using the same NMR data but in the context of a more comprehensive quadruple force field search (i.e., with AMBER*, MMFFs, MM3*, and OPLS 2005, each supplemented with the GBSA/H_2O continuum solvent model). The conceptors of the NAMFIS methodology have pointed out that conformational deconvolution is ideally conducted in the context of a complete set of conformations,[9] a condition difficult to achieve with a single method applied to a complex natural product. As structural variables in the present reanalysis, 40 interatomic proton−proton distances from a 2D ROESY treatment[18] and 14 three-bond coupling constants ($^3J_{H-H}$) were used for the study.

NAMFIS analysis combining the NMR data and the 1282 conformers gave 12 best-fit conformations (NAMFIS 1-NAMFIS 12, SSD[10,19] = 49) with populations ranging from 2 to 17%. The significance of this conformational ensemble is highlighted by the fact that the single X-ray conformer alone yields the considerably higher SSD[19] of 246, indicating it to be a rather poor fit to the data by comparison with the 12 conformer pool. The top three NAMFIS conformations are illustrated in Figure 3.

Inspection of the 12 conformations indicates many defining characteristics. The conformers can be divided into four classes; X-ray (58%), sickle (17%), dome (17%), and extended (9%). Seven out of 12 are internally hydrogen bonded, with five sustaining a hydrogen bond between a hydroxyl on the main chain or the lactone and the carbamate side chain. Such intramolecular H-bonds in DMSO are well-known[20] and are believed to be able to compensate for a *syn*-pentane interaction.[21] Five conformations including NAMFIS-2 (14%) and NAMFIS-3 (12%) display the lactone in a boat conformation with all substituents equatorial. Many of the NAMFIS conformers also share similarity with each other. For instance, NAMFIS-5 (10%), NAMFIS-9 (4%), and NAMFIS-12 (2%) superpose very well (Figure 4), as do NAMFIS-3 (12%) and NAMFIS-8 (5%). The principal difference among these conformations is found in the butenyl side chain and the orientation of the lactone, whereas for most of them the C5−C18 sections overlap closely.

Comparison of many of the NAMFIS conformers with the X-ray conformation indicates a surprising similarity between them, especially in the C5−C18 segment. For example the X-ray conformer superposes very well with NAMFIS-12 (2%), NAMFIS-5 (10%), and NAMFIS-4 (12%), as illustrated in Figure 5.

Overall, 8 out of 12 NAMFIS structures superpose with the X-ray conformation in the C5−C18 region with rmsd values of less than 1 Å, and four of these overlap with values of less than 0.5 Å. The main conformational variability exists

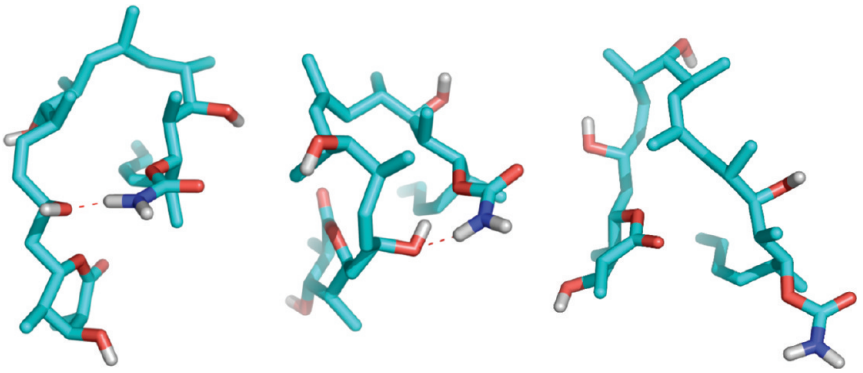

Figure 3. Top three NAMFIS conformational families of DDM in DMSO-d_6. From left: sickle 17%; dome 17%, and X-ray 58%, respectively. The top two clusters sustain a hydrogen bond between the carbamate NH_2 and the C-7 hydroxyl.

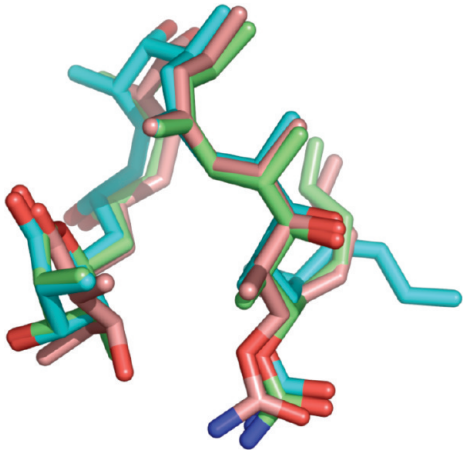

Figure 4. Overlap of NAMFIS-5 (blue), NAMFIS-9 (pink), and NAMFIS-12 (green). The average heavy-atom rmsd is 0.5 A.

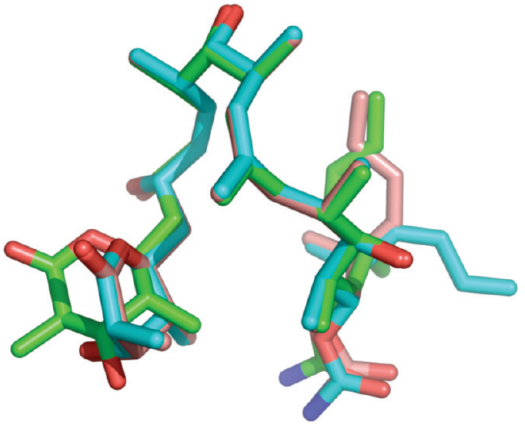

Figure 5. Overlap of the X-ray conformation (green) with NAMFIS-5 (blue) and NAMFIS 12 (pink); rmsd = 0.4 Å.

in the butenyl and lactone side chains. As noted above, because the X-ray structure is very similar to the force field global minima, the aforementioned NAMFIS conformers also overlap closely with the global minima. In terms of percentage, 58% of conformers in DMSO-d_6 are part of the X-ray family, while 42% fall into other structural clusters. The dominance of the X-ray family contrasts with our preliminary study[18] in which no more than 1% of the conformations resembled the X-ray conformation. Thus, the current evaluation emphasizes that multiple force field searching[22] maps the conformational surface for DDM more comprehensively and provides a substantially different result from a single force field search. The largest change, of course, is the emergence of the hairpin form as overriding consistent with other experimental approaches. However, similar families are also located in both the studies. The best fit conformation in the present investigation, for instance, belongs to the second-most dominant "sickle" family in the previous single force field study.

Torsional Clustering and Coupling Constant Analysis in DMSO-d_6. While the NAMFIS procedure provides a comprehensive overview of a complex conformational equilibrium, other more reductionist approaches likewise deliver valuable conformational insights from an alternative perspective. For example, in solution studies of epothilones, torsional clustering of computed conformer pools followed by comparison with experimental data has permitted important structural deductions.[23,24] At a reviewer's request, the two approaches have been compared in the context of the NAMFIS conformer pool.

Accordingly, the NAMFIS conformers were clustered around the H10−C10−C11−H11 and H11−C11−C12−H12 dihedral angles with Schrodinger's Maestro (see Methods) by choosing one conformer and aligning other rotamers to it by heavy-atom superposition as monitored by rms deviation.[25] The choice of these angles arises from their centrality within the DDM structure and the resulting influence on the overall shape of the molecule, particularly the hairpin geometry. Clustering reveals four distinct molecular shapes. Of 12 NAMFIS conformers, eight belong to the first cluster and present the monitored dihedrals in the hairpin g−/a conformation comprising 58% of the conformational ensemble as described above. Two minima belong to the second cluster with g−/g+ geometry (dome). The remaining two structures represent the final clusters with a/a and g+/a conformations (sickle and extended, respectively). Overall, torsional angle clustering is in excellent agreement with the interpretation depicted in Figure 3 and Table 1. From this analysis, however, one might conclude that there are only four distinct conformations instead of 12 as deduced from the NAMFIS approach. However, this exercise has treated only two key torsional angles at the bend junction of the molecule. When viewed in terms of the remaining torsions, particularly at the DDM lactone and diene termini (Figure 4), the richness of the conformational variation becomes apparent. This illustrates that a full analysis of the torsional surface of a molecule of DDM's complexity requires a method such as NAMFIS that simultaneously processes all of the NMR data against a large set of conformations.

Table 1. Percentages of NAMFIS-Derived DDM Populations in DMSO-d_6 and D_2O and Their Classification into X-Ray and Non-X-ray Families

conformer no.	% DMSO-d_6	% D_2O	family in D_2O	family in DMSO-d_6
1	17	12	X-ray	sickle
2	14	11	X-ray	dome
3	12	10	X-ray	X-ray
4	12	10	dome	X-ray
5	10	9	X-ray	X-ray
6	9	8	X-ray	X-ray
7	9	7	X-ray	extended
8	5	4	sickle	X-ray
9	4	4	X-ray	X-ray
10	4	4	X-ray	X-ray
11	3	3	dome	dome
12	2	3	X-ray	X-ray
13		2	X-ray	
14		2	dome	
15		2	X-ray	
16		2	X-ray	

The second related approach is the evaluation of conformation−activity relationships as developed by Taylor et al. in the context of epothilone conformation.[26] A combination of NMR-derived vicinal coupling constants ($^3J_{H-H}$) and molecular modeling led to identification of two interconverting conformational families in solution. With regard to DDM, ^3J(H10−H11) and ^3J(H11−H12) were measured as 2.2 and 8.8 Hz, respectively.[27] The first value implies a gauche relationship, while the latter predicts a torsion somewhat below that of the ideal anticonformation (i.e., 165−170°). Why is this value found to be 8.8 and not 9−10 Hz, diagnostic of a torsion angle closer to 180°? It can be understood by examining the $^3J_{H-H}$ values calculated from the H10−H11 and H11−H12 dihedral angles of the 12 NAMFIS conformations. Eleven H10−H11 values lie between 0.6 and 2.0 Hz, while one falls at 9.7 Hz. Similarly, for H11−H12, 10 of the couplings reside in the 9.0−9.8 Hz range, corresponding to pure anticonformers (X-ray, sickle), while two are present at 0.6 and 0.5 Hz (dome). The Supporting Information provides the explicit values. The population-weighted averages of the two sets of coupling constants are 2.2 and 8.5 Hz, respectively. The dominant conformation with respect to the fulcrum angles is the hairpin shape with g−/a geometry (Figure 4). A similar treatment applies to H16−H17 and H17−H18 torsion angles with $^3J_{H-H}$ values observed at 7.8 and 2.3 Hz, respectively.[27] This analysis illustrates that a few deviant conformers in a rapidly equilibrating set can lead to the impression that nonideal geometries are permitted based on averaged J values. Deconvolution, however, reveals that significantly different low energy local minimum geometries are present in the equilibrium. The geometric mix delivers composite observables that characterize no one conformation completely. Seen from this viewpoint, the measured coupling constants are fully consistent with the preponderance of hairpin g−/a structures depicted in Figures 1−5.

Conformational Distribution in D_2O. The percentage of conformers belonging to the X-ray family increases substantially in water. Using the distance and coupling constant data from Canales et al.,[6] we analyzed DDM conformations in D_2O using NAMFIS (SSD 194) and found that 80% of the conformers belong to the X-ray family. However, the number of distinct rotational isomers located in water (16) is greater than that in DMSO (12). Examination of the structures from both solvents reveals similarities. For instance, an identical conformer from the X-ray family is found in DMSO-d_6 (9%) and D_2O (2%). Similarly, sickle (17% and 4%, respectively) and dome (17% and 13%, respectively) families are found in both solvents. The extended family is present only in DMSO-d_6. However the X-ray family clearly dominates in both solvents as it does in CD_3CN.[8] Table 1 reports the percentages of conformers in both data sets and classifies them into X-ray and non-X-ray ensembles. The criterion used to classify a conformer as belonging to the X-ray family is a C5−C19 heavy atom rmsd of 0.5 Å or less. These observations indicate that solvent changes, in this case from polar aprotic to protic, result in a redistribution of major conformer families without altering the essential nature of the individual conformations.[28]

Clearly, there is a dominant and energetically stable hairpin conformation for the C5−C18 segment of discodermolide that emerges in solution, as a global minimum in multiple force field conformational searches and in the solid state. As discussed below, this motif is also similar to the proposed bioactive conformation.

The Origin of the Hairpin DDM Conformation. To pinpoint the energetic source of the persistent torsional characteristics of the hairpin geometry, we focus on the C5−C18 region with the reasonable assumption that the conformational mobility of the more flexible carbamate and lactone side chains (Figures 4 and 5) has little influence on it. At the same time, we draw inspiration from the pioneering work of Hoffmann and co-workers who have investigated *syn*-pentane interactions in substituted pentane and related systems.[12,13]

To suppress the influence of electrostatic effects that frequently dominate conformational preferences in force field conformational searches,[14] the carbamate side chain was excised subsequent to evaluating steric aspects of the resulting molecule. In a first calculation, we replaced the hydroxyls at positions 7, 11, and 17 with methyl groups. Multiple force-field conformational searches (MM3, MMFFs, OPLS 2005, AMBER) with this structure demonstrated the global minima to be very similar to those for the parent DDM molecule. A similar outcome was achieved by replacing the three hydroxyls with hydrogens. Superpositions of these minima with the X-ray conformation are provided in Figure 6.

To further explore the conformational preferences in individual sectors of the molecule, we simplified the conformational profiles and performed OPLS2005 conformational searches with short nonpolar fragments of the discodermolide backbone consisting of the C6−C24, C7−C17, and C12−C24 regions. As before, the global minima for these structural fragments match closely the corresponding sectors of DDM as shown in Figure 7.

The composite results indicate that the energetic preferences for discodermolide arise mainly from steric factors and are preserved in individual segments of the molecule. It is noteworthy that DDM incorporates three methyl-hydroxy-methyl units, which have been exploited as symmetrical synthons in the many convergent syntheses of discodermolide reported.[4c] While they are convenient synthetic elements, this triplet of synthons likewise clearly determines the conformation of the molecular backbone of DDM. These results are in complete accord with the deductions of Hoffman,[12,13] while emphasizing that

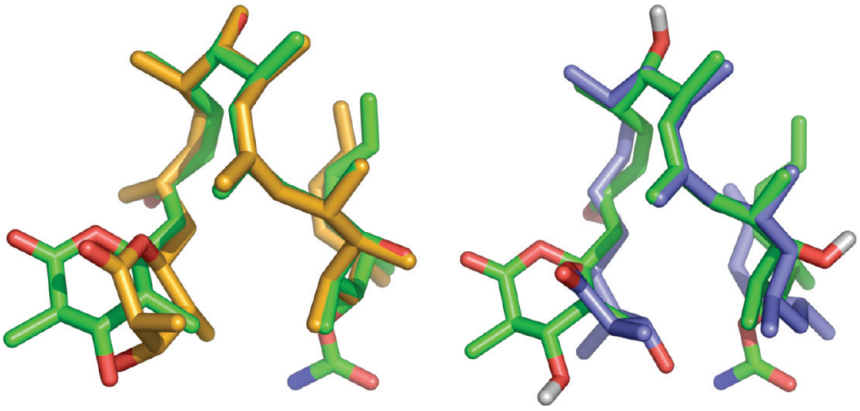

Figure 6. Overlap of the DDM X-ray conformation (green) with carbamate excised fragment global minima. Left: C-7, C-11, and C-17 hydroxyls replaced by methyl groups; right: C-7, C-11, and C-17 hydroxyls removed.

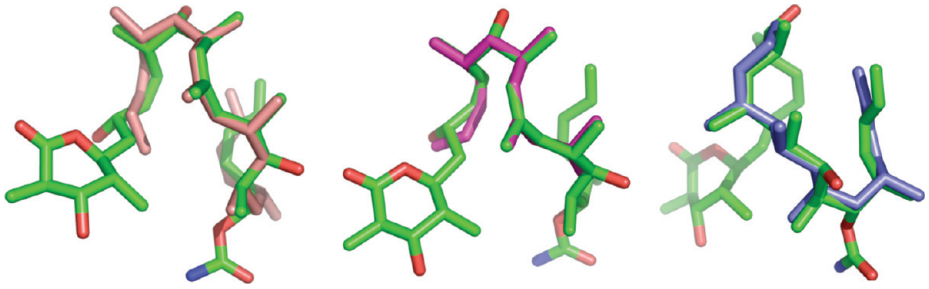

Figure 7. Superpositions of the global minima for the C6−C24, C7−C17, and C12−C24 fragment structures (from left to right) of DDM with the X-ray conformation (green).

sequential appearances of substituted pentanes in a molecular architecture can result in an overwhelming preference for a given conformation in spite of the presence of numerous easily rotated single bonds. Further support for this assertion is provided in the Supporting Information.

The Tubulin-Bound Conformation of DDM. Two groups have applied Tr-ROESY and related NMR techniques to determine a tubulin-bound conformation for DDM. Sanchez-Pedregal et al.[5] proposed a model for the latter employing a soluble form of tubulin and first suggested the bound geometry to be similar to the solid-state and solution conformations of the same ligand. More recently, Canales et al.[6] confirmed the hairpin conformer as the protein-bound entity in the presence of guanosine 5′-(α,β-methylenetriphosphate)-enriched tubulin present as 92−95% solubilized microtubules, concluding that only minor differences obtain between conformers derived from the two tubulin preparations, most notably in the disposition of the butenyl group. As described above, the same study also derived the hairpin conformer as the primary conformation in water. Thus, both studies suggest a common 3-D geometry shared by solid-state, solution, and protein-bound environments. By contrast, our investigation indicates a distribution of DDM conformations in solution with the proposed bound conformation represented as a dominant geometry among them. Figure 8 exhibits the overlap between the solid-state, NAMFIS-10, and protein-bound[6] conformations (ave C5−C18 rmsd 0.5 A).

Interestingly, in the Canales et al. study,[6] the conformer providing the fit to the NMR variables is a global minimum on the MM3* potential energy surface. In the present work, the global minima from the AMBER*, MMFFs, and OPLS-2005 searches were also similar to the MM3* global minimum. However, in solution, because a nontrivial fraction of the NAMFIS conformations (e.g., NAMFIS-1, 2 and 3) are dissimilar to the proposed bound conformation, there would appear to be a much greater degree of conformational selection during the binding event than suggested by the previous two reports.

The Binding Mode of DDM in Tubulin. A binding model for DDM based on the shape and structure of the taxane binding pocket in β-tubulin (PDB code 1JFF) has been reported recently by Canales et al. using AUTODOCK (Pose-1).[6] Considering the lack of direct structural information and the importance of the drug, we elected to reexamine potential DDM poses with Glide,[29] RosettaLigand,[30] and AUTODOCK (v 4.0).[31] Both of the latter examine the flexibility of the side chains within the binding site. Because the binding form of DDM has been determined to be in the hairpin conformation by elegant NMR studies of the tubulin−DDM complex,[5,6] all dockings were performed with DDM constrained to the coordinates derived by the Canales group (Figure 8).[6] In each of the docking experiments, initial docking poses were rescored with MM-GBSA energies.[32]

The top 20 Glide and RosettaLigand poses included Pose-1 (Figure 9) and a number of others that score better dependent on the docking method used. However, rescoring with MM-GBSA asserts that Pose-1 is the lowest energy among them and, therefore, favored. On the other hand, AUTODOCK generated 100 poses for DDM, which were clustered into three categories. MM-GBSA rescoring of the lowest energy member of each cluster gave relative ΔG values of −14, −22 (Pose-1), and −28 (Pose-2) kcal/mol. The latter best scoring binding mode, like Pose-1, locates DDM close to the crucial M-loop implicated in the interactions between tubulin protofilaments in microtubules. Both poses are also

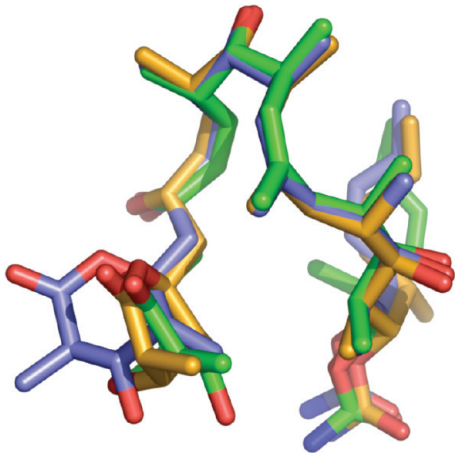

Figure 8. Overlap of DDM tubulin-bound (golden), X-ray (green), and NAMFIS-10 (blue) conformations.

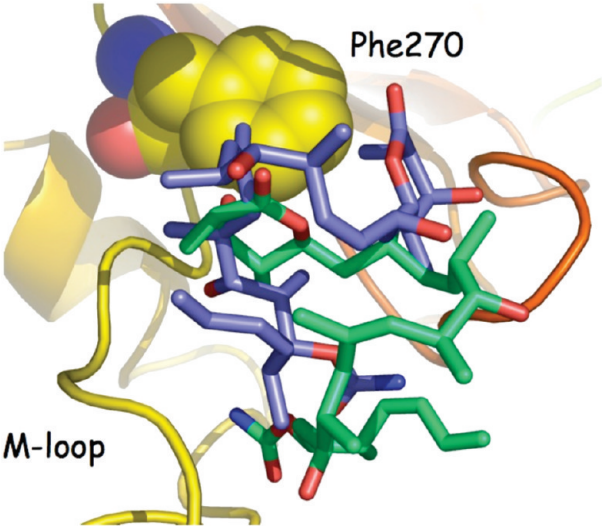

Figure 9. Canales et al.[6] Pose-1 (blue) and the best MM-GBSA scored AUTODOCK Pose-2 (green). The relative positions arise from superposing the β-tubulin−DDM complexes. The M-loop is depicted in yellow.

situated at a distance from Phe272, an observation consistent with the noninvolvement of this residue in ligand binding as deduced from the activity of DDM against paclitaxel resistant cell lines[33] and SAR data on dictyostatin analogues.[34] Relative orientations of the two poses resulting from superposition of the corresponding β-tubulin−DDM complexes are depicted in Figure 9.

Differences in the two favored poses illustrate alternative anchoring in the binding cleft while maintaining intimate contact with the M-loop. In Pose-1, the C12−C17 sector constituting the hairpin turn faces the M-loop. The O17 hydroxyl oxygen of DDM makes a hydrogen bond with Thr274 of the M-loop, while the C12 and C16 methyl groups form a hydrophobic cluster with Leu273. At the ligand's lactone terminus, the O7−Gly360 hydrogen bond is complemented with a C4−Leu361 nonpolar contact (Figure 10).

By contrast, the MM-GBSA favored Pose-2 directs the termini of the hairpin DDM conformer toward the M-loop (Figure 11). It makes three widely spaced hydrogen bonds from O3, N19, and O17 to M-loop residues Pro272, Thr274,

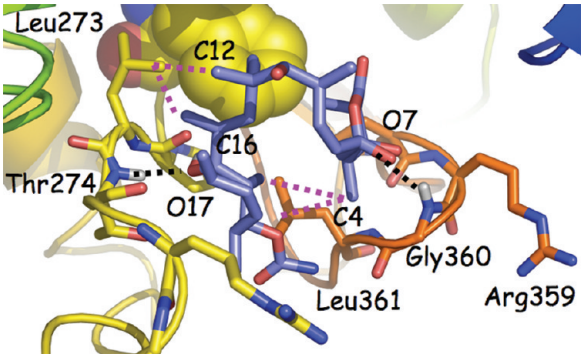

Figure 10. Canales et al. Pose-1 illustrating the major contacts (H-bonds black dotted lines; hydrophobic contacts magenta dotted lines) with the M-loop (yellow) and the adjacent loop (orange) linking β-strands B9 and B10.

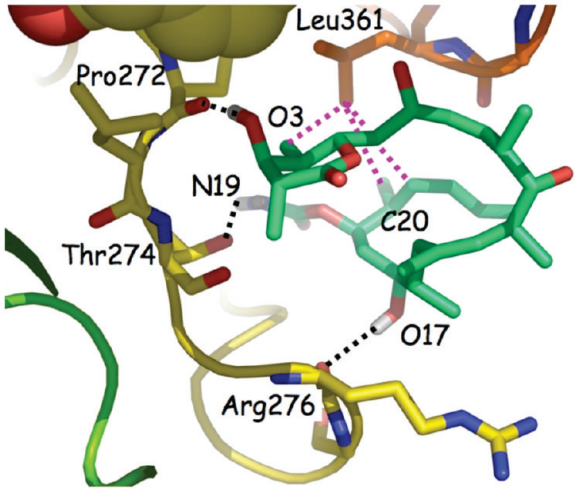

Figure 11. MM-GBSA favored AUTODOCK Pose-2 illustrating the major polar (black dotted lines) and nonpolar (magenta dotted lines) contacts with the M-loop (yellow) and the adjacent loop (orange) linking β-strands B9 and B10.

and Arg276, respectively. In addition, topologically, C4 and C20 methyl groups and the C21−C22 double bond form a productive hydrophobic cluster with Leu361 of the loop connecting B9 and B10 (Figure 11).

It would be remiss to leave this issue without mentioning the previous work of Martello et al.,[16] which took a ligand-based rather than a receptor-based approach to suggesting two DDM−tubulin binding models, one of which was favored (model I). These were derived from the lower resolution PTX/β-tubulin complex (pdb code 1TUB) augmented with the crystal structure of the polar conformation of PTX.[35] In particular, the C-19 and δ-lactone moieties of the hairpin discodermolide structure were superposed in two separate orientations on the C-2 and C-13 side chains of PTX/1TUB within a pocket defined by Asp224, His227, Thr274, and Gly368. Not surprisingly, because these models drew inspiration from an early supposition proposing the polar conformation of PTX[36] to be tubulin-bound rather than the now well-established T-Taxol form,[37] they bear little relationship to the receptor-based poses depicted in Figures 10 and 11.

Poses 1 and 2 and DDM Structure−Activity Relationships. There are three aspects to the SAR of (+)-discodermolide

as it relates to binding its primary tubulin/microtubule cellular target: (1) cell lines resistant to paclitaxel and other taxane site ligands by virtue of mutations in β-tubulin; (2) modifications of DDM that disrupt the hairpin conformation or leave it intact, and (3) substituent variations that sustain the bioactive conformation but either enhance or diminish compound potency by virtue of ligand−side chain interactions within the binding pocket. We present selected aspects of DDM SAR from categories (1−3) to illustrate that, while a number of DDM modifications can be rationalized by both Pose-1 and Pose-2 (Figure 9), certain structural variations are only accommodated by Pose-2 (i.e. category 3).

(+)-Discodermolide is cytotoxic at nanomolar concentrations when exposed to paclitaxel resistant ovarian carcinoma cell lines (1A9PTX10 and 1A9PTX22)[33] and epothilone B resistant human lung carcinoma cells (A549-t12).[4g,38] Tubulin in these cell lines harbors mutations at Phe270Val, Ala364Thr, and Gln292Glu, respectively, near the taxane binding site. However, the atomic separations between these residues and the DDM ligand in Poses 1 and 2 (Figures 9−11) range from 3.8 (Phe270) to 7 Å (Gln292) accounting for the lack of cross-resistance and the ineffectiveness of these mutations to ablate DDM action.

In the analyses for (2) and (3) to follow, we do not consider biological effects mediated by P-glycoprotein efflux pumps. However, we make the simplifying assumption that, to a first approximation, cellular potency can be rationalized by considering the hairpin structure as the biologically active form, which undergoes only modest conformational deformation in response to chemical manipulation when bound to microtubular tubulin. While membrane permeability effects and differential solubilities may strongly influence the SAR correlation in some cases, key biostructural trends as mirrored by the poses of Figure 9 can nonetheless be identified.

First, we examine structural variants of DDM (**1**) that compromise the hairpin conformer, taking the comprehensive SAR reviews of Smith and Freeze[4c] and Shaw[4g] as the source of summaries of the experimental data. Most of the described conformational disruptions have been substantiated by explicit modification of Pose-1 followed by geometry optimization with the MMFF force field. In one striking observation, configurational interconversion of the *Z*-olefin at C8−C9[16] to the *E*-geometry leads to significant loss of potency. A *trans*-C8−C9 isomer simply cannot sustain the U-shaped organization shown in Figure 1 because its locus is nearly a third of the way down the molecular backbone. The same can be predicted for the *trans*-C13−C14 olefin at the halfway point along the backbone, although this variant does not appear to have been prepared. Synthesis of an approximate surrogate for the latter at Novartis involved moving the rigid and planar "olefinic" unit one carbon further along the backbone by replacing the C14−C15 single bond with an *N*-methyl amide.[4c] This change alters the C13═C14−C15−C16 torsion angle from ∼120° to a value of either 0 or 180° (i.e., C13−N(Me)−C(═O)−C16). Because the 119° angle assists in maintaining spatial separation between the C1−C9 and C16−C24 legs of the hairpin conformer, amide flattening occasions cross-leg contacts, and conformational reorganization. Not surprisingly, the amide exhibits micromolar activity in four of five cell lines tested as compared with DDM's 6−10 nM action in the same cells.

A third example concerns the complete loss of cell growth inhibition upon epimerization of the C17−OH center.[39] In the hairpin conformer, the C17−H to H−C22 distance is at the lower van der Waals limit for a pair of nonbonded protons (2.2 Å). Inversion at C17 leads to severe O17---H−C22 crowding and the unfolding of the hairpin. Acetylation of either C11 or C17 likewise causes a striking reduction in activity[4c,40] that can be attributed to a steric clash between the acetyl moiety and the C12 and C18 methyl groups, respectively, with concomitant deformation of the hairpin geometry. Epimerization at C7 likewise leads to 1−2 orders of magnitude activity loss for several cell lines.[4c,40] Short contacts within the hairpin structure between C7−OH and C10−H are consistent with consequent affinity-ablating conformational reorganizations.

Finally, an important modification of DDM that simplifies the synthesis of several series of analogues is the elimination of the methyl group at C14.[16] In many cases, cell growth inhibition is unaffected by the latter excision when compared with **1**.[41] The hairpin conformer exhibits no close intramolecular contacts with this CH_3, suggesting it contributes little to conformational stability. In both Pose-1 and Pose-2, the C14−CH_3 shows minimal hydrophobic contacts with protons of single residues: His227 (ring CH, 2.4 Å) and Arg276 (side chain δ-CH, 2.3 Å) respectively. Thus, C14 methyl depletion is compatible with the biostructural environments of both ligand and the surrounding protein. The same can be said for discarding the C16 methyl group to give the 16-normethyl analogue, which retains low nanomolar potency.[40] In the two binding models of Figure 9, only single hydrophobic contacts are observed from the protein to C16-Me, the loss of which would not appear to influence binding affinity significantly. On the other hand, epimerization at C16 causes a 50-fold reduction in potency.[40] This can be attributed to conformational scrambling, because the C16−CH_3---O−C17 separation in the hairpin architecture would fall well below the sum of van der Waals radii, while a classic *syn*-pentane clash would arise between C14 and C16 methyl groups.

With respect to other DDM−protein interactions, an unusual series of experimental observations reveals that the lactone ring can be deprived of substituents or replaced by ring surrogates such as valerolactone, butyrolactone, phenol and coumarin without a serious impact on biological activity.[16,41−43] In some cases, substituent-depleted analogues gave a 3−7 fold activity improvement. Both binding models (Figures 9-11) accommodate these results. Pose-1 places the lactone in a region of the β-tubulin pocket bounded largely by hydrophobic residues (Val23, His227, Ala231, Phe270, Pro358, alkyl chain of Arg359, Gly360, Leu361), as does Pose-2 (Leu215, His227, Phe270, Pro272, Leu273). Accordingly, a flat and somewhat characterless hydrophobic ring is viewed as capable of anchoring the DDM architecture into the binding pocket in the context of both models. Smith and Freeze[4c] have argued that the placement and orientation of the C-1 lactone carbonyl is critical for driving potency. While neither model provides a direct hydrogen bond to this center, both place the His227 NH within 3−4 Å of the carbonyl oxygen. A water-bridge between the centers (N−H---O-(H)-H---O═C1) readily accommodates a structural role for the carbonyl moiety.

A revealing trio of lactone replacements is captured in structures **3** and **4**. The 7-substituted coumarin **3** and the corresponding C23−C24 saturated analogue deliver antiproliferation profiles virtually identical to parent DDM.[43c] However, the 6-substituted analogue **4** exhibits a 60−70-fold reduction in activity.

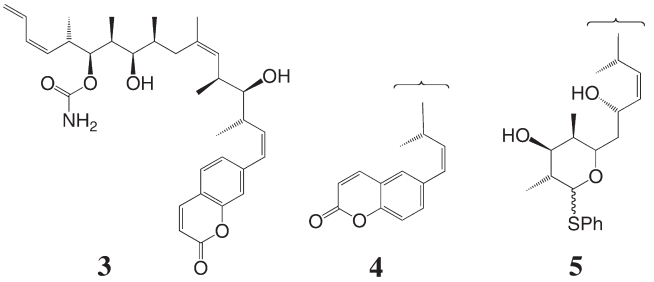

3 **4** **5**

Glide docking of **3** and its C23−C24 saturated analogue constrained as the hairpin conformation into the tubulin binding pocket delivers Pose-2, while Pose-1 is predicted to be much less favored. Isomer **4** also docks as Pose-2, but locates the lactone C=O away from His227 in a hydrophobic patch bounded by Leu217, Phe272, Leu230. The lack of electrostatic complementarity rationalizes the basis for its low activity.

The epimers of the C1 thiophenyl acetals **5** and the corresponding nor-C16 analogue all show tumor cell growth suppression equivalent to DDM (~5 nM). These highly active analogues provide another diagnostic for distinguishing the two poses. Each of the acetals were Glide-docked into the protein, but only Pose-2 accommodates the bulky substituents of both C1 stereoisomers. No satisfying variation of Pose-1 could be identified because the SPh groups in this binding mode would penetrate the protein framework.

Turning to the lactone C3−OH, each of the two DDM poses (1 and 2) portrays a well-defined hydrogen bond from the alcohol center. Pose-1 predicts the OH to be a proton acceptor (C3−O---HN H-bond with Gly360 at 2.2 Å), while Pose-2 depicts a proton donor (C3−OH---O=C Pro272 at 1.73 Å). The finding that the C3−OH group on the lactone ring is not required for activity (2,3-anhyrodiscodermolide,[16,44] 3-methoxy, and 3-deoxy[45] discodermolides are active at single digit nanomolar concentrations) reinforces the idea that a hydrophobic environment surrounding the ring offers a significant affinity contribution willing to sacrifice directed hydrogen bonding. Thus, a hydrogen bond to C3−OH appears to add little to the orientation of the ligand in the binding site, while remaining energetically neutral as a result of a compensating H-bond in solution.

Two other substituent trends provide insights into the binding models for DDM. First the addition of bulky groups to the C23−C24 terminal olefin is tolerated without a deleterious effect on bioactivity. Both the photoaffinity tag **6**[46] and the linker in **7**[40] provide DDM analogues with low nM potency. The C24 extension of **7** is tolerated only by Pose-2, which locates the pivaloyl-terminated moiety at the entrance to the ligand pocket (Figure 9). Pose-1, on the other hand, positions the diene in the vicinity of Leu217 and Leu219. Elongation directs the alkOPiv group into conflict with the protein, preventing effective binding in this ligand orientation.

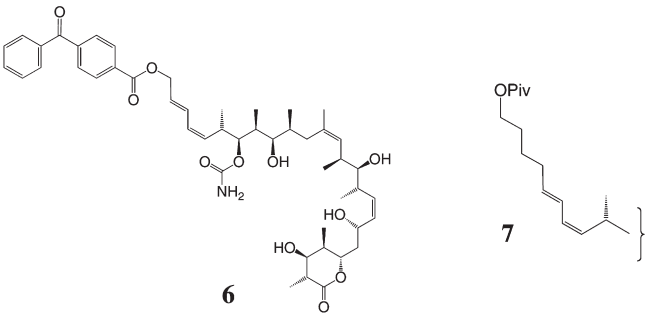

6 **7**

Second, large polar and apolar alkyl and aryl groups can be installed at the NH_2 of the C-19 carbamate with little drop in potency for many analogues in sensitive cell lines (e.g., **8**−**10**).[47] The compounds either rival (+)-discodermolide or improve its activity in several cell lines. The present DDM−tubulin models rationalize the potency by presenting proton donors suitable for H-bonding or π-stacking in the M-loop region occupied by the terminal groups (Pose-1: Arg282 and Lys362; Pose-2: Ala283 NH and Tyr281).

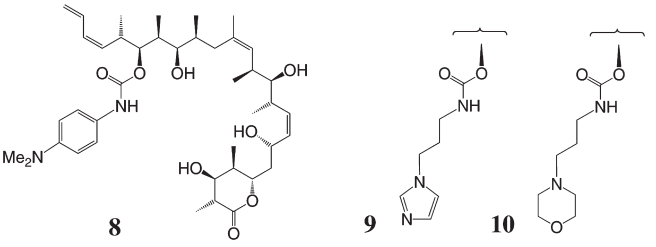

8 **9** **10**

Conclusions and Outlook

In summary, a multiple force field and NAMFIS solution analysis of discodermolide has been performed to provide a realistic and high quality fit of the NMR data obtained in DMSO-d_6 to an ambient solution ensemble of conformations. The molecule adopts a strongly preferred conformation with respect to the central sector of the molecule. Conformational analysis aided by force field and quantum chemical calculations underscores the notion that steric factors stabilize the latter in three separate environments: solution, the solid-state, and in the tubulin binding site. However, studies on other flexible, bioactive molecules suggest that the ligand-only X-ray structure is commonly influenced by crystal packing factors. Likewise, a protein-bound conformer is anchored by still another set of noncovalent forces. As a result, both ligand crystal structures and bioactive conformers are often minor, but identifiable components of the conformational ensemble in solution where such effects are absent.[21] In general, NAMFIS solution studies on tubulin ligands such as PTX[37a] and epothilone-A[48] have identified the bioactive conformation as a minor solution ensemble component.

Discodermolide would appear to be a significant exception to the latter generalization due to the presence of the three rigidifying fragments containing tandem vicinal Me, OH, and Me functionality. Relatively straightforward steric factors seem to influence the existence of a common dominant conformer in different surroundings. This is

rarely the case, because differential energetic requirements ordinarily lead to conformational diversity among the microenvironments.[21] In the present instance, however, the overriding conformational preference induced largely by steric factors (i.e., $A^{1,3}$ strain and *syn*-pentane interactions[8,12,13]) leads to a dominant 3D form under all three circumstances. Insofar as the conformational preferences of DDM dictate the latter under very different physical conditions, the methyl-hydroxy-methyl triad and related moieties suggest themselves as modular, Lego-like elements that permit straightforward application of molecular mechanics-guided conformational principles to prediction of the bioactive conformations of related natural and synthetic products. Such approaches may also suggest synthetic design strategies incorporating multiple appearances of the modular component to impose conformational preferences in addition to offering synthetic advantage as in the Smith group convergent synthesis of (+)-discodermolide.[4c,7]

The combined conformational and NAMFIS analyses also indicate that simplified versions of discodermolide, for example ones in which the hydroxyls are removed or replaced by methyls or ones in which certain portions of the chain are excised or substituted by other groupings, may sustain the DDM conformational preferences. Such truncated constructs, by preserving binding interactions driven by the adoption of a favorable molecular shape, can possibly provide improved drug-like properties, thereby enhancing therapeutic utility.

Finally, docking of DDM in the tubulin binding site complemented by MM-GBSA calculations has identified a second binding pose (Pose-2). Comparative analysis of the latter and the previously reported Pose-1 illustrates that both models accommodate a range of the data. However, a subset of the SAR, in particular lactone and diene substitution, is compatible only with Pose-2. Further studies will be needed to substantiate this proposal definitively. Nonetheless, the present models may well offer inspiration in the pursuit of active, bioavailable and side-effect free DDM analogues.[49]

Methods

Conformational Searches. Conformational searches were performed in Macromodel[50] (Schrodinger, v7.2)[51] with four force fields; AMBER*, MMFFs, MM3*, and OPLS 2005 using 40000 structure generation steps, an energetic cutoff of 7 kcal/mol, and the GBSA/H_2O continuum solvent model.[52] The mixed low mode/MCMM method[53] was used for searching and the truncated Newton conjugate gradient procedure for structure optimization. In each case, the global minimum was found at least 15 times, indicating that the conformational surface had been exhaustively sampled.[54] The resulting structures from each individual force field search were brought to full convergence with a final Newton−Raphson optimization step, after which the structures from each search were combined and duplicates were eliminated. The resulting structure pool was submitted to NAMFIS analysis as input.

NAMFIS. The NAMFIS methodology has been described in detail elsewhere.[9,10,22] In its optimal application, NAMFIS takes as its input a set of optimized structures from a "complete" conformational search and a set of averaged three bond $^3J_{H-H}$ coupling constants and interatomic proton distances from 1D and 2D NOESY NMR spectra, respectively. The NMR data used in this work was previously gathered in DMSO-d_6.[18] In sum, NAMFIS performs a least-squares fitting of the averaged NMR variables and the corresponding calculated parameters for the conformation pool and thereby derives a Boltzmann population of conformations that together comprehensively fit the NMR data. Goodness of fit is expressed as the sum of squares differences (SSD)[10,19] with a lower SSD indicating a better fit.[55]

Docking. As a preliminary to docking, the $\alpha\beta$-tubulin dimer (pdb code 1JFF) was "prepared" in Maestro 8.5.207 by adding hydrogens, assigning bond orders, and subjecting the structure to optimization applied to nonbonded interactions with OPLS-2005. Subsequently, a standard precision (SP) rigid Glide (v 3.5)[29] docking was performed using the DDM structure as derived by Canales et al.[6] All settings for grid generation and SP docking were default. The grid was centered on the native paclitaxel ligand in 1JFF. A Prime MM-GBSA[32] energy evaluation was then performed on the 20 Glide poses using default settings. In the structure activity analysis, additional atom-freezing was performed for common atoms in DDM and DDM derivatives prior to optimization with OPLS2005 followed by Glide docking.

For RosettaLigand[30] docking, the Maestro-prepared tubulin was reduced to β-tubulin, the paclitaxel ligand was removed, and the ligand coordinates were used to define six different starting points using standard default values. DDM was docked as a rigid body into the protein, and 1000 docking poses were analyzed to select the 20 top poses as scored by RosettaLigand. These ligand−protein poses were subjected to Prime MM-GBSA energy scoring.

For AutoDock[31] treatment, the Maestro-prepared tubulin was reduced to β-tubulin and the Taxol and GTP ligands were removed. The DDM ligand and protein were imported into AutoDockTools (ADT v 1.4.5), and ADT was employed for ligand and protein preparation for compatibility with Autodock. A grid was constructed to encompass the empty paclitaxel binding site and parametrized using Autogrid4. A total of 100 docking poses were generated using Autodock4 using default settings for both Autogrid and Autodock. The 100 poses were clustered using ADT, and the lowest energy docking pose from each cluster was rescored using Prime MM-GBSA.

Density Functional Theory (DFT) Calculations. Single-point quantum chemical DFT energy evaluations of conformers of force-field optimized 2,3,4-trisubstituted-pentane analogues were performed at the B3LYP/6-31G* level with Schrodinger's Jaguar quantum chemical package. See the Supporting Information for the relative energies of low energy conformations.

Acknowledgment. We are grateful to Professor Jesús Jiménez-Barbero (CIB-CSIC, Madrid, Spain) for sharing the coordinates of DDM bound to β-tubulin in Pose-1 (Figures 9 and 10) and to Pieter B. Burger (South African exchange fellow) for assistance in coordinate interconversion. We are likewise appreciative to Professor Dennis C. Liotta (Emory University) for encouragement and support.

Supporting Information Available: Coupling constant deconvolution and DFT evaluation of 2,3,4-trisubstituted-pentanes. This material is available free of charge via the Internet at http://pubs.acs.org.

References

(1) Gunasekera, S. P.; Gunasekera, M.; Longley, R. E.; Schulte, G. K. Discoderolide: A New Bioactive Polyhydroxylated Lactone from the Marine Sponge *Discodermia dissoluta*. *J. Org. Chem.* **1990**, *55*, 4912–4915.

(2) Buey, R. M.; Barasoain, I.; Jackson, E.; Meyer, A.; Giannakakou, P.; Paterson, I.; Mooberry, S.; Andreu, J. M.; Diaz, J. F. Microtubule Interactions with Chemically Diverse Stabilizing Agents: Thermodynamics of Binding to the Paclitaxel Site Predicts Cytotoxicity. *Chem. Biol.* **2005**, *12*, 1269–1279.

(3) Mita, A.; Lockhart, A.; Chen, T. A phase I pharmacokinetic (PK) of AAA296A (discodermolide) administered every 3 weeks in adult

patients with advanced solid tumors. *Proc. Am. Soc. Clin. Oncol.* **2004**, *23*, 133(Abstr 2025) .

(4) (a) Mollat du Jourdin, X.; Noshi, M.; Fuchs, P. L. Designer Discodermolide Segments via Ozonolysis of Vinyl Phosphonates. *Org. Lett.* **2009**, *11*, 543–346. (b) de Lemos, E.; Porée, F. H.; Bourin, A.; Barbion, J.; Agouridas, E.; Lannou, M. I.; Commerçon, A.; Betzer, J. F.; Pancrazi, A.; Ardisson, J. Total Synthesis of Discodermolide: Optimization of the Effective Synthetic Route. *Chem.—Eur. J.* **2008**, *14*, 11092–11112. (c) Smith, A. B.; Freeze, B. S. (+)-Discodermalide: Total Syntheses, Construction of Novel Analogues, and Biological Evaluation: An Overview. *Tetrahedron* **2008**, *64* (2), 261–298. (d) Paterson, I.; Naylor, G. J.; Wright, A. E. Total synthesis of a potent hybrid of the anticancer natural products dictyostatin and discodermolide. *Chem. Commun.* **2008**, *38*, 4628–4630. (e) Florence, G. J.; Gardner, N. M.; Paterson, I. Development of practical syntheses of the marine anticancer agents discodermolide and dictyostatin. *Nat. Prod. Rep.* **2008**, *25*, 342–375. (f) Cao, H.; Parker, K. A. Short Synthesis of the C1−C14 Stretch of Discodermolide from Building Blocks Prepared by Asymmetric Catalysis. *Org. Lett.* **2008**, *10*, 1353–1356. (g) Shaw, S. J. The Structure−Activity Relationship of Discodermolide Analogues. *Mini-Rev. Med. Chem.* **2008**, *8*, 276–284.

(5) Sanchez-Pedregal, V. S.; Kubicek, K.; Meiler, J.; Lyothier, I.; Paterson, I.; Carlomagno, T. The Tubulin-Bound Conformation of Discodermolide Derived by NMR Studies in Solution Supports a Common Pharmacophore Model for Epothilone and Discodermolide. *Angew. Chem., Int. Ed.* **2006**, *45*, 7388–7394.

(6) Canales, A.; Matesanz, R.; Gardner, N. M.; Andreu, J. M.; Paterson, I.; Diaz, J. F.; Jiménez-Barbero, J. The Bound Conformation of Microtubule-Stabilizing Agents: NMR Insights into the Bioactive 3D Structure of Discodermolide and Dictyostatin. *Chem.—Eur. J.* **2008**, *14*, 7557–7569.

(7) Smith, A. B.; Beauchamp, T. J.; LaMarche, M. J.; Kaufman, M. D.; Qiu, Y.; Arimoto, H.; Jones, D. R.; Kobayashi, K. Evolution of a Gram-Scale Synthesis of (+)-Discodermolide. *J. Am. Chem. Soc.* **2000**, *122*, 8654–8664.

(8) Smith, A. B.; LaMarche, M.; Falcone-Hindley, M. Solution Structure of (+)-Discodermolide. *Org. Lett.* **2001**, *3*, 695–698.

(9) Cicero, D. O.; Barbato, G.; Bazzo, R. NMR Analysis of Molecular Flexibility in Solution: A New Method for the Study of Complex Distributions of Rapidly Exchanging Conformations. Application to a 13-Residue Peptide with an 8-Residue Loop. *J. Am. Chem. Soc.* **1995**, *117*, 1027–1033.

(10) Nevins, N.; Cicero, D. O.; Snyder, J. P. A Test of the Single-Conformation Hypothesis in the Analysis of NMR Data for Small Polar Molecules: A Force Field Comparison. *J. Org. Chem.* **1999**, *64*, 3979–3986.

(11) Mickel, S. J.; Niederer, D.; Daeffler, R.; Osmani, A.; Kuesters, E.; Schmid, E.; Schaer, K.; Gamboni, R.; Chen, W.; Loeser, E.; Kinder, F. R., Jr.; Konigsberger, K.; Prasad, K.; Ramsey, T. M.; Repic, O.; Wang, R.-M.; Florence, G.; Lyothier, I.; Paterson, I. Large-Scale Synthesis of the Anti-Cancer Marine Natural Product (+)-Discodermolide. Part 5: Linkage of Fragments C_{1-6} and C_{7-24} and Finale. *Org. Process Res. Dev.* **2004**, *8*, 122–130and cited references. .

(12) Hoffmann, R. W.; Stahl, M.; Shopfer, U.; Frenking, G. Conformation Design of Hydrocarbon Backbones: A Modular Approach. *Chem.—Eur. J.* **1998**, *4*, 559–566.

(13) Hoffmann, R. W.; Stenkamp, D.; Trieselmann, T.; Gottlich, R. Flexible Molecules with Defined Shape XI Conformer Equilibria in 2,4-Disubstituted Pentane Derivatives. *Eur. J. Org. Chem.* **1999**, 2915–2917.

(14) Lakdawala, A.; Wang, M.; Nevins, N.; Liotta, D. C.; Rusinska-Rosak, D.; Lozynski, M.; Snyder, J. P. Calculated Conformer Energies for Organic Molecules with Multiple Polar Functionalities are Method Dependent: Taxol Case Study. *BMC Biology* **2001**, *1*, 2.

(15) As pointed out by Martello et al. (ref 16), the distributed X-ray coordinates of (+)-discodermolide require mirror-image inversion to correspond to the absolute configuration of the natural product.

(16) Martello, L. A.; LaMarche, M. J.; He, L.; Beauchamp, T. J.; Smith, A. B., III; Horwitz, S. B. The relationship between Taxol and (+)-discodermolide: synthetic analogs and modeling studies. *Chem. Biol.* **2001**, *8*, 843–855.

(17) Perola, E.; Charifson, P. S. Conformational Analysis of Drug-Like Molecules Bound to Proteins: An Extensive Study of Ligand Reorganization upon Binding. *J. Med. Chem.* **2004**, *47*, 2499–2510.

(18) Monteagudo, E.; Cicero, D. O.; Cornett, B.; Myles, D. C.; Snyder, J. P. The Conformations of Discodermolide in DMSO. *J. Am. Chem. Soc.* **2001**, *123*, 6929–6930.

(19) SSD = sum of square differences between the measured and modeled geometric variables; i.e. the NOE derived H---H interatomic distances and the dihedral angle defining 3-bond coupling constants, $^3J_{H-H}$. The smaller the value, the better the fitting. Good to excellent fits between data and structure ordinarily fall at SSD < 100. For the analytical expression used to evaluate the latter, see refs 9 and 10.

(20) (a) Kondo, M. Spectroscopic Studies of Solvent Effects on Intramolecular Hydrogen Bonding in *N*-Substituted Salicylamides. *Bull. Chem. Soc. Jpn.* **1979**, *52*, 521–523. (b) Nazir, H.; Yildiz, M.; Tahir, M. N.; Uikü, D. Intramolecular hydrogen bonding and tautomerism in Schiff bases. Structure of N-(2-pyridil)-2-oxo-1-naphthylidenemethylamine. *J. Mol. Struct.* **2000**, *524*, 241–250. (c) Crisp, G. T.; Jiang, Y.-L. Intramolecular hydrogen bonding of (+)-biotin and biotin derivatives in organic solvents (DC-178BP). *ARKIVOC* **2001**, *vii*, 77–87. (d) Ko, H.; Shim, G.; Kim, Y. Evidences that β-Lactose Forms Hydrogen Bonds in DMSO. *Bull. Korean Chem. Soc.* **2005**, *26*, 2001–2006.

(21) Thepchatri, P.; Cicero, D. O.; Monteagudo, E.; Ghosh, A. K.; Cornett, B.; Liotta, D. C.; Snyder, J. P. Relationship Among Ligand Conformations in Solution, in the Solid State, and at the Hsp90 Binding Site: Geldanamycin and Radicicol. *J. Am. Chem. Soc.* **2005**, *127*, 12838–12846.

(22) Thepchatri, P.; Eliseo, T.; Cicero, D. O.; Myles, D.; Snyder, J. P. Conformations of Laulimalide in DMSO-d_6. *J. Am. Chem. Soc.* **2007**, *129*, 3127–3134.

(23) (a) Taylor, R. E.; Zajicek, J. Conformational Properties of Epothilone. *J. Org. Chem.* **2000**, *64*, 7224–7228. (b) Taylor, R. E.; Zajicek, J. Correction. *J. Org. Chem.* **2000**, *65*, 5449.

(24) Erdélyi, M.; Pfeiffer, B.; Hauenstein, K.; Fohrer, J.; Gertsch, J.; Altmann, K.-H.; Carlomagno, T. Conformational Preferences of Natural and C3-Modified Epothilones in Aqueous Solution. *J. Med. Chem.* **2008**, *51*, 1469–1473.

(25) The maximum average heavy atom rmsd for conformations in any one cluster is 0.6 Å.

(26) Taylor, R. E.; Chen, Y.; Galvin, G. M.; Pabba, P. K. Conformation−activity relationships in polyketide natural products. Towards the biologically active conformation of epothilone. *Org. Biomol. Chem.* **2004**, *2*, 127–132.

(27) ref 18, Supporting Information.

(28) A similar NAMFIS analysis of DDM in acetonitrile[8] using geometric variables presented by Canales et al.[6] reveals an even higher percentage (84%) of the X-ray-like conformation (data not shown). However, because the interproton distances representing the CD_3CN experiment were derived from a single proposed MM3* conformation,[6] we consider this result to be only an approximation to the unpublished NMR data.

(29) (a) Friesner, R. A.; Banks, J. L.; Murphy, R. B.; Halgren, T. A.; Klicic, J. J.; Mainz, D. T.; Repasky, M. P.; Knoll, E. H.; Shaw, D. E.; Shelley, M.; Perry, J. K.; Sander, L. C.; Shenkin, P. S. Glide: A New Approach for Rapid, Accurate Docking and Scoring. 1. Method and Assessment of Docking Accuracy. *J. Med. Chem.* **2004**, *47*, 1739–1749. (b) Halgren, T. A.; Murphy, R. B.; Friesner, R. A.; Beard, H. S.; Frye, L. L.; Pollard, W. T.; Banks, J. L. Glide: A New Approach for Rapid, Accurate Docking and Scoring. 2. Enrichment Factors in Database Screening. *J. Med. Chem.* **2004**, *47*, 1750–1759.

(30) Davis, I. W.; Baker, D. ROSETTALIGAND Docking with Full Ligand and Receptor Flexibility. *J. Mol. Biol.* **2009**, *385*, 381–392.

(31) (a) Morris, G. M.; Goodsell, D. S.; Halliday, R. S.; Huey, R.; Hart, W. E.; Belew, R. K.; Olson, A. J. Automated Docking Using a Lamarckian Genetic Algorithm and and Empirical Binding Free Energy Function. *J. Comput. Chem.* **1998**, *19*, 1639–1662. (b) Huey, R.; Morris, G. M.; Olson, A. J.; Goodsell, D. S. A Semiempirical Free Energy Force Field with Charge-Based Desolvation. *J. Comput. Chem.* **2007**, *28*, 1145–1152.

(32) (a) Niu, H.; Kalyanaraman, C.; Irwin, J. J.; Jacobson, M. P. Physics-Based Scoring of Protein−Ligand Complexes: Enrichment of Known Inhibitors in Large-Scale Virtual Screening. *J. Chem. Inf. Model.* **2006**, *46*, 243–253. (b) Lyne, P. D.; Lamb, M. L.; Saeh, J. C. Accurate Prediction of the Relative Potencies of Members of a Series of Kinase Inhibitors Using Molecular Docking and MM-GBSA. *J. Med. Chem.* **2006**, *49*, 4805–4808. (c) Graves, A. P.; Shivakumar, D. M.; Boyce1, S. E.; Jacobson, M. P.; Case, D. A.; Shoichet, B. K. Rescoring Docking Hit Lists for Model Cavity Sites: Predictions and Experimental Testing. *J. Mol. Biol.* **2008**, *377*, 914–934.

(33) Kowalski, R. J.; Giannakakou, P.; Gunasekera, S. P.; Longley, R. E.; Day, B. W.; Hamel, E. The microtubule-stabilizing agent discodermolide competitively inhibits the binding of paclitaxel (Taxol) to tubulin polymers, enhances tubulin nucleation reactions more potently than paclitaxel, and inhibits the growth of paclitaxel-resistant cells. *Mol. Pharmacol.* **1997**, *52*, 613–622.

(34) Jung, W. H.; Harrison, C.; Shin, Y.; Fournier, J. H.; Balachandran, R.; Raccor, B. S.; Sikorski, R. P.; Vogt, A.; Curran, D. P.; Day, B. W. Total Synthesis and Biological Evaluation of C16 Analogs of (−)-Dictyostatin. *J. Med. Chem.* **2007**, *50*, 2951–2966.

(35) Mastropaolo, D.; Camerman, A.; Luo, Y.; Brayer, G. D.; Camerman, N. Crystal and Molecular Structure of Paclitaxel (Taxol). *Proc. Natl. Acad. Sci. U.S.A.* **1995**, *92*, 6920–6924.
(36) Li, Y.; Poliks, B.; Cegelski, L.; Poliks, M.; Gryczynski, Z.; Piszczek, G.; Jagtap, P. G.; Studelska, D. R.; Kingston, D. G. I.; Schaefer, J.; Bane, S. REDOR NMR Distance Measurements for the Tubulin-Bound Paclitaxel Conformation. *Biochemistry* **2000**, *39*, 281–291.
(37) (a) Snyder, J. P.; Nettles, J. H.; Cornett, B.; Downing, K. H.; Nogales, E. The binding conformation of Taxol in β-tubulin: A model based on electron crystallographic density. *Proc. Natl. Acad. Sci. U.S.A.* **2001**, *98*, 5312–5316. (b) Paik, Y.; Yang, C.; Metaferia, B.; Tang, S.; Bane, S.; Ravindra, R.; Shanker, N.; Alcaraz, A. A.; Snyder, J. P.; Cegelski, L.; Kingston, D. G. I. Rotational-Echo Double-Resonance NMR Distance Measurements for the Tubulin-Bound Paclitaxel Conformation. *J. Am. Chem. Soc.* **2007**, *129*, 361–370. (c) Ganesh, T.; Yang, C.; Norris, A.; Glass, T.; Bane, S.; Ravindra, R.; Shanker, N.; Banerjee, A.; Metaferia, B.; Thomas, S. L.; Giannakakou, P.; Alcaraz, A. A.; Lakdawala, A. S.; Snyder, J. P.; Kingston, D. G. I. Evaluation of the Tubulin-Bound Paclitaxel Conformation: Synthesis, Biology and SAR Studies of C-4 to C-3′ Bridged Paclitaxel Analogs. *J. Med. Chem.* **2007**, *50*, 713–725.
(38) Yang, C.-P. H.; Verdier-Pinard, P.; Wang, F.; Lippaine-Horvath, E.; He, L.; Li, D.; Hofle, G.; Ojima, I.; Orr, G. A.; Horwitz, S. B. A highly epothilone B-resistant A549 cell line with mutations in tubulin that confer drug dependence. *Mol. Cancer Ther.* **2005**, *4*, 987–995.
(39) Hung, D. T.; Nerenberg, J. B.; Schreiber, S. L. Syntheses of Discodermolides Useful for Investigating Microtubule Binding and Stabilization. *J. Am. Chem. Soc.* **1996**, *118*, 11054–11080.
(40) Kinder, F. R., Jr.; Bair, K. W.; Chen, W.; Florence, G. J.; Francavilla, C.; Geng, P.; Gunasekera, S.; Lassota, P. T.; Longley, R.; Palermo, M.; Paterson, I.; Pomponi, S.; Ramsey, T. M.; Rogers, L.; Sabio, M.; Sereinig, N.; Sorensen, E.; Wang, R.; Wright, A. Global SAR study of the novel microtubule stabilizing agent discodermolide. *Proc. AACR* **2002**, *43*, 3650; Presented at American Association for Cancer Research 93rd Annual Meeting, San Francisco, CA, 2002. Poster no. 3650. .
(41) Smith, A. B., III; Freeze, B. S.; LaMarche, M. J.; Hirose, T.; Brouard, I.; Xian, M.; Sundermann, K. F.; Shaw, S. J.; Burlingame, M. A.; Horwitz, S. B.; Myles, D. C. Design, Synthesis, and Evaluation of Analogues of (+)-14-Normethyldiscodermolide. *Org. Lett.* **2005**, *7*, 315–318.
(42) (a) Kinder, F. R. Process For Preparing Discodermolide And Analogues Thereof. Patent WO 2,002,012,220, **2002**; (b) Kinder, F. R., Jr.; Kapa, P. K.; Loeser, E. M. Certain Salts Of Discodermolide Acid, Pharmaceutical Compositions Containing Them and Their Use In Treating Tumors. Patent WO 2,002,098,843, **2002**; (c) Kinder, F. R., Jr.; Bair, K. W.; Ramsey, T. M.; Sabio, M. L. Certain Substituted Polyketides, Pharmaceutical Compositions Containing Them And Their Use In Treating Tumors. Patent WO 2,003,014,102, **2003**.
(43) (a) Burlingame, M. A.; Shaw, S. J.; Sundermann, K. F.; Zhang, D.; Petryka, J.; Mendoza, E.; Liu, F.; Myles, D. C.; LaMarche, M. J.; Hirose, T.; Freeze, B. S.; Smith, A. B., III. Design, synthesis and cytotoxicity of 7-deoxy aryl discodermolide analogues. *Bioorg. Med. Chem. Lett.* **2004**, *14*, 2335–2338. (b) Shaw, S. J.; Sundermann, K. F.; Burlingame, M. A.; Myles, D. C.; Freeze, B. S.; Xian, M.; Brouard, I.; Smith, A. B., III. Toward Understanding How the Lactone Moiety of Discodermolide Affects Activity. *J. Am. Chem. Soc.* **2005**, *127*, 6532–6533. (c) Shaw, S. J.; Menzella, H. G.; Myles, D. C.; Xian, M.; Smith, A. B., III. Coumarin-derived discodermolide analogues possessing equivalent antiproliferative activity to the natural product—a further simplification of the lactone region. *Org. Biomol. Chem.* **2007**, *5*, 2753–2755.
(44) Gunasekera, S. P.; Longley, R. E.; Isbrucker, R. A. Semisynthetic Analogues of the Microtubule-Stabilizing Agent Discodermolide: Preparation and Biological Activity. *J. Nat. Prod.* **2002**, *65*, 1830–1837.
(45) Shaw, S. J.; Sundermann, K. F.; Burlingame, M. A.; Zhang, D.; Petryka, J.; Myles, D. C. A series of 23,24-dihydrodiscodermolide analogues with simplified lactone regions. *Bioorg. Med. Chem. Lett.* **2006**, *16*, 1961–1964.
(46) Smith, A. B., III; Rucker, P. V.; Brouard, I.; Freeze, B. S.; Xia, S.; Horwitz, S. B. Design, Synthesis, and Biological Evaluation of Potent Discodermolide Fluorescent and Photoaffinity Molecular Probes. *Org. Lett.* **2005**, *7*, 5199–5202.
(47) Smith, A. B., III; Freeze, B. S.; LaMarche, M. J.; Hirose, T.; Brouard, I.; Rucker, P. V.; Xian, M.; Sundermann, K. F.; Shaw, S. J.; Burlingame, M. A.; Horwitz, S. B.; Myles, D. C. Design, Synthesis, and Evaluation of Carbamate-Substituted Analogues of (+)-Discodermolide. *Org. Lett.* **2005**, *7*, 311–314.
(48) Nettles, J. H.; Li, H.; Cornett, B.; Krahn, J. M.; Snyder, J. P.; Downing, K. H. The Binding Mode of Epothilone A on α, β-Tubulin by Electron Crystallography. *Science* **2004**, *305*, 866–869.
(49) Atomic coordinates for Pose-1 are available from Professor Jesús Jiménez-Barbero (ref 6); Pose-2, from the present authors upon request.
(50) Mohamadi, F.; Richards, N. G. J.; Guida, W. C.; Liscamp, R.; Lipton, M.; Caufield, C.; Chang, G.; Hendrickson, T.; Still, W. C. MacroModel—an integrated software system for modeling organic and bioorganic molecules using molecular mechanics. *J. Comput. Chem.* **1990**, *11*, 440–467.
(51) Schrödinger, Inc., 120 West 45th Street, 29th Floor, New York, NY 10036−4041, +1 (646) 366−9555, http://www.schrodinger.com/.
(52) Still, W. C.; Tempczyk, A.; Hawley, R.; Hendrickson, T. Semianalytical treatment of solvation for molecular mechanics and dynamics. *J. Am. Chem. Soc.* **1990**, *112*, 6127–6129.
(53) Kolossvary, I.; Guida, W. C. Low Mode Search. An Efficient, Automated Computational Method for Conformational Analysis: Application to Cyclic and Acyclic Alkanes and Cyclic Peptides. *J. Am. Chem. Soc.* **1996**, *118*, 5011–5019.
(54) Chang, G.; Guida, W. C.; Still, W. C. An internal-coordinate Monte Carlo method for searching conformational space. MCMM. *J. Am. Chem. Soc.* **1989**, *111*, 4379–4386.
(55) Kelso, M. J.; Beyer, R. L.; Hoangt, H. N.; Lakdawala, A. S.; Snyder, J. P.; Oliver, W. V.; Robertson, T. A.; Appleton, T. G.; Fairlie, D. P. α-Turn Mimetics: Short Peptide α-Helices Composed of Cyclic Metallopentapeptide Modules. *J. Am. Chem. Soc.* **2004**, *126*, 4828–4842.